Opto-Electronic Advances

ISSN 2096-4579 CN 51-1781/TN

Speckle structured illumination endoscopy with enhanced resolution at wide field of view and depth of field

Elizabeth Abraham, Junxiao Zhou and Zhaowei Liu

Citation: Abraham E, Zhou JX, Liu ZW. Speckle structured illumination endoscopy with enhanced resolution at wide field of view and depth of field. *Opto-Electron Adv* **6**, 220163(2023).

https://doi.org/10.29026/oea.2023.220163

Received: 10 October 2022; Accepted: 6 March 2023; Published online: 6 May 2023

Opto-Electronic Advances

Article

July 2023, Vol. 6, No. 7

DOI: 10.29026/oea.2023.220163

Speckle structured illumination endoscopy with enhanced resolution at wide field of view and depth of field

Elizabeth Abraham, Junxiao Zhou and Zhaowei Liu*

Structured illumination microscopy (SIM) is one of the most widely applied wide field super resolution imaging techniques with high temporal resolution and low phototoxicity. The spatial resolution of SIM is typically limited to two times of the diffraction limit and the depth of field is small. In this work, we propose and experimentally demonstrate a low cost, easy to implement, novel technique called speckle structured illumination endoscopy (SSIE) to enhance the resolution of a wide field endoscope with large depth of field. Here, speckle patterns are used to excite objects on the sample which is then followed by a blind-SIM algorithm for super resolution image reconstruction. Our approach is insensitive to the 3D morphology of the specimen, or the deformation of illuminations used. It greatly simplifies the experimental setup as there are no calibration protocols and no stringent control of illumination patterns nor focusing optics. We demonstrate that the SSIE can enhance the resolution 2–4.5 times that of a standard white light endoscopic (WLE) system. The SSIE presents a unique route to super resolution in endoscopic imaging at wide field of view and depth of field, which might be beneficial to the practice of clinical endoscopy.

Keywords: speckle structured illumination endoscopy; wide field of view; large depth of field; easy-to-implement; low cost

Abraham E, Zhou JX, Liu ZW. Speckle structured illumination endoscopy with enhanced resolution at wide field of view and depth of field. *Opto-Electron Adv* **6**, 220163 (2023).

Introduction

Endoscopy is an optical imaging technique that has been widely practiced across the globe since the nineteenth century. Image quality here is of utmost importance, both for examination and diagnosis. There are many parameters that determine optimal image quality. Resolution is one such important metric, critical for endoscopic practices[1–3]. This metric quantifies details in frames that are otherwise not visible to the naked eye without proper processing. Resolution in an optical system is principally limited by its diffraction limit. Therefore, overcoming the diffraction limit and achieving super resolution of an optical system has been a very dynamic research field for the last two decades.

There are several super resolution imaging techniques practiced prevalently in the field of microscopy. Stochastic optical reconstruction microscopy (STORM) and photo activated localization microscopy (PALM) are single molecule localization-based methods that bring optical resolution down to sub-10 nm scales[4,5]. However, they suffer from very slow imaging speeds. On the other hand, stimulated emission depletion (STED), is faster and has a good video rate[6]. However, the field of view is limited due to its point-by-point scanning approach. In

Department of Electrical and Computer Engineering, University of California, San Diego, 9500 Gilman Drive, La Jolla, California 92093, United States.

*Correspondence: ZW Liu, E-mail: zhaowei@ucsd.edu

Received: 10 October 2022; Accepted: 6 March 2023; Published online: 6 May 2023

addition, it needs exceptionally high laser intensity and complex instrumentation. Although traditional structured illumination microscopy (SIM), can only improve the resolution by 2-fold compared to the diffraction limit, it has been widely applied in bioimaging[7,8]. This wide field method can be operated under low intensity and high speeds. Recently, high resolution SIM technologies have been demonstrated by introducing plasmonics and metamaterials into SIM[9–12]. Many variant super resolution techniques have also been developed by the combination of multiple methods mentioned above.

Despite the remarkable success, most of the super resolution microscopy techniques cannot be directly extended to the field of endoscopy. In a standard white light endoscope (WLE), the hardware used includes imaging and illumination optics which must be well confined within the endoscope's distal tip. This means only compact optics that does not affect the size of the distal tip is allowed. In addition, large field of view, large depth of field and focus-free optics is required in endoscopic applications. Although high resolution endoscopic methods exist, they have significant limitations. One of the prominent high-resolution techniques that has been clinically used in gastrointestinal imaging is called confocal laser endomicroscopy (CLE)[13,14]. The CLE works by illuminating the tissue with a laser source and detecting the reflected fluorescent light from the tissue through a confocal aperture. Analogous to confocal laser microscopy, CLE is a scanning technique with a narrow field of view, typically in micrometers[15–17]. Here the depth of field can be precisely selected at a time, but it is challenging to obtain a stereoscopic image with high speed. Hence, a comprise is commonly encountered in resolution vs. the field of view and depth of field. This may result in higher rates of sampling errors which inevitably leads to undesired complications[18,19]. A limited field of view at the cost of good resolution could also entail increased screening and operational time, cost, and a potential risk to the patient[20–24]. To overcome these limitations, we need a robust method that can achieve high resolution simultaneously with a large field of view and depth of field.

Compared to other super resolution methods, SIM has the best potential to be applied in endoscopy due to its wide field and high-speed nature. In traditional SIM, known spatially structured patterns of light, like periodic fringes, are used to excite the sample. The spatial frequency mixing of the object and the illumination patterns occurs. Spatial mixing encodes structural details corresponding to the high spatial frequency of the sample into detectable low spatial frequency Moiré fringes[25–28]. Therefore, high frequency components which are otherwise lost by conventional imaging techniques can be effectively recovered. A super resolution image of SIM is reconstructed through an image reconstruction algorithm using a series of low-resolution frames with different illumination patterns. The resolution of SIM can be determined by an effective numerical aperture (*NA*) given by

$$NA_{\rm SIM} = NA_{\rm ill} + NA_{\rm det}\ , \tag{1}$$

where $NA_{\rm ill}$ and $NA_{\rm det}$ represent the effective *NA* of illumination and detection optics, respectively. Traditional SIM utilizes the same optics for illumination and detection. This results in a resolution improvement of about twofold.

However, traditional SIM technologies emphasize absolute resolution so that optics with very high NA is used. This inevitably leads to very small depth of field which is not suitable for endoscopy. Additionally, well-defined illumination patterns in standard SIM can only be well predicted on a planar object plane. They become distorted, blurred, and unpredictable when they are projected onto an arbitrary and unknown 3D surface. This results in the loss of known illumination patterns. Recovering the image without prior knowledge of the illumination pattern can be overcome by using blind-SIM algorithm with a constraint that all the illumination patterns add up to a uniform intensity. This concept was demonstrated and called the speckle illumination technique[29–34]. Speckle SIM is highly tolerable to illumination distortion as it is based on the statistical nature of the speckles. If we can separate the illumination and the image optics, with a fixed imaging system, the resolution would be primarily limited by the speckle resolution, thus, the overall speckle SIM resolution improvement factor may go far beyond twofold.

In this work, we propose and demonstrate a novel super resolution endoscopic technique called speckle structured illumination endoscopy (SSIE) to overcome the limitations described. This modality is aimed to achieve wide field, high resolution, and large depth of field in images. Unlike CLE, we do not make any modifications to the existing WLE's image collection hardware, rather, we introduce an external light source from which the illumination patterns are transmitted and routed via multimode fibers onto the target. The advantage of using

WLE's imaging optics is that it offers a larger field of view and depth of field compared to CLE. The super resolution capability of the SSIE is brought about by the blind-SIM algorithm that makes use of the high-resolution speckle patterns projected onto the sample, hence, eliminating the dependence of resolution on the imaging optics of the endoscopic system. We prove the SSIE concept using fluorescence imaging on both 2D and 3D surfaces. Depending on the image distance, the SSIE resolution shows 2–4.5 times improvement compared to a standard WLE modality.

Working principle of SSIE

In this section we describe the working principle of SSIE. A standard surveillance WLE has distal and proximal ends with two main integral elements, namely the illumination source and the acquisition system. The illumination source in WLE is traditionally comprised of either lamps or LEDs which are routed from the proximal end to the distal end through the fiber bundles and onto the target[35]. The acquisition system typically placed at the distal end, contains a couple of channels which include the air, water and biopsy ports, and the imaging optics which consists of a wide-angle objective lens and the image sensor[36]. In SSIE, we retain all the components of a WLE, but add two multi-mode fibers along the insertion tube from an external low power laser. The idea here is to create a system where the clinician can switch between the incoherent illumination mode of the WLE and the coherent illumination mode of the SSIE as needed. The schematic of SSIE is shown in Fig. 1 emphasizing the additional components to a traditional WLE system.

In SSIE, a continuous wave (CW) low power laser (can be any wavelength but we select 532 nm as an example in this work) is coupled into a fiber collimator (objective of fiber launch: 40×/0.65*NA*). This optical field is directed into a fiber beam splitter via a speckle generator (e.g., a length of fiber with a vibrational motor). The speckle is controlled by the vibrational motor attached to the fiber spool which will stretch the fiber and change the interfering phase during image acquisition (see Supplementary information for more details). The fiber beam splitter couples the light into two identical multi-mode fibers surrounding the endoscope tube as shown in Fig.1. The incident optical field is scrambled due to the multi-mode interference and can be changed by adding vibration to the fiber. The two multimode fibers are placed on either ends of the endoscope so that large angle interference of random speckles is formed containing high spatial frequency components beyond the diffraction limit of the image collection optics. The high-resolution information of the object is detected through frequency mixing of the object and the illumination speckles. Multiple frames of the object with these high-resolution speckles are captured and used for the final image reconstruction.

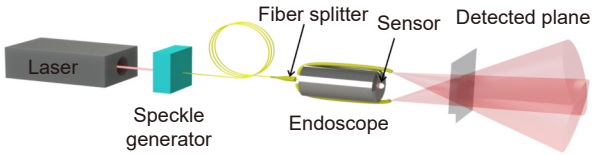

Fig. 1 | Schematic of SSIE. A continuous wave laser is routed through two multimode fibers via speckle generator onto the object. The intrinsic image sensor of the endoscope is used to collect images.

Based on the SSIE configuration shown in Fig. 2(a), we first simulated two exemplary speckle illumination patterns and their Fourier transforms which are depicted in Fig. 2(b) and 2(c). Clearly, the speckle resolution decreases with the distance. As the two fibers are placed along the y axis, the interference pattern along the y axis also shows slightly higher resolution.

As illustrated in Fig. 2(a), the two fibers are tilted towards the optical axis of the endoscope to ensure sufficiently large overlap for the interference area and cover the entire field of view (FOV) of a WLE at various focal depths. Since the NA of the fibers can be selected to be much larger than that of the detection optics, it is fairly easy to identify an appropriate tilt angle of the fibers, so that the interference area may fully cover the whole endoscope's field of view. Assuming $P(x_2, y_2, d)$ is an arbitrary location in the object plane, the spatial frequency of interference pattern at P is determined by $2k_0\sin\alpha/2$, where k_0 is the wavevector of the laser light in free space, and α is the angle between the two-interfering light (see Fig. 2(a)). The angle α can be expressed as:

$$\alpha = \arccos\left(\frac{\boldsymbol{r}_1\cdot\boldsymbol{r}_2}{|r_1||r_2|}\right) = \arccos\left(\frac{x_2^2+y_2^2-\frac{w^2}{4}+d^2}{\sqrt{x_2^2+\left(y_2-\frac{w}{2}\right)^2+d^2}\cdot\sqrt{x_2^2+\left(y_2+\frac{w}{2}\right)^2+d^2}}\right), \tag{2}$$

where w is the width of the endoscope. Applying the paraxial approximation, i.e., $d>>x_2, y_2$, the above equation

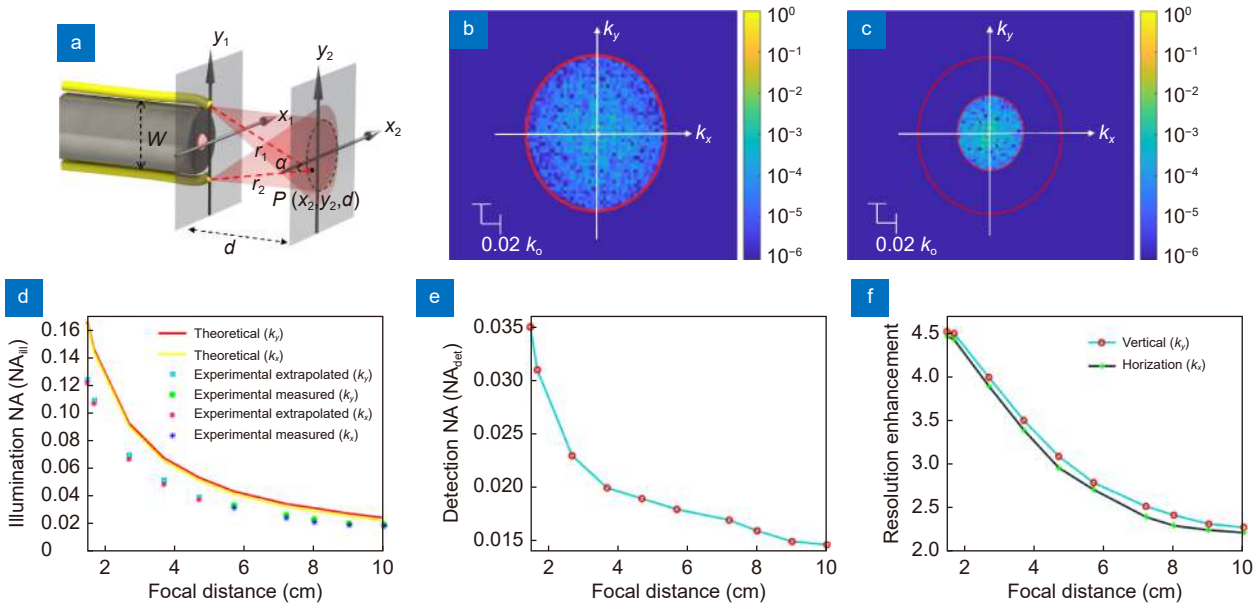

Fig. 2 | Characterization of the speckle patterns and the estimated resolution enhancement of SSIE compared to traditional WLE. (**a**) Schematic of the endoscope with illumination projected at distance *d*. The field of view should be covered by light from both fibers. (**b**, **c**) Numerical simulated Fourier spectra of the speckle patterns at *d*=3.7 cm and *d*=7.2 cm, respectively. (**d**) Theoretical and experimental illumination NA (NA_{ill}) for various distances *d* from 1.5 to 10 cm. Focal distance 5.7–10 cm (measured); 1.5–5.7 cm (extrapolation was performed with a power trendline as an exponential curve). (**e**) Experimentally detected NA (NA_{det}) for different focal distance *d*. (**f**) Estimated SSIE resolution enhancement factor compared to traditional WLE at various focal distances.

becomes $\alpha=\arccos\left(\frac{4d^2-w^2}{4d^2+w^2}\right)=\arccos\left(1-\frac{2w^2}{4d^2+w^2}\right)$. From Eq. (2), and its simplified form, we observe that α drops with an increase in distance d, which indicates closer the sample to the endoscope, more of the high frequency components of the illumination patterns will be utilized. We measured the speckle patterns using a CCD camera at different distance d, and the deduced and extrapolated effective illumination NA is summarized in Fig. 2(d). These results agree reasonably well with our numerical simulations, and the slightly low values in experiment are likely due to the low dynamic range of the CCD camera. To identify the detection NA (NA_{det}) in accordance with Eq. (1), we calibrate the endoscopic system against the standard USAF (United States Air Force Target) target (see more information in the Supplementary information). The experimentally calibrated values of NA_{det} are in Fig. 2(e). The SSIE resolution enhancement factor compared to traditional WLE is given by

$$\frac{(NA_{ill}+NA_{det})}{NA_{det}}, \tag{3}$$

and the estimated values are presented in Fig. 2(f), where a resolution enhancement of 2-4.5-fold is achievable. The placement of the fibers enables the large angle interference of the modulated speckle patterns which produces a high NA than that of the endoscopic detection NA, surpassing its diffraction limit as shown in Fig. 2(d, e). Notice the slightly different enhancement factors along x, and y axis, which is consistent with the asymmetrical Fourier spectra shown in Fig. 2(b) and 2(c). Such large resolution enhancement factors originate from the fine interreference illumination patterns. Using a single fiber source without interference will result in the NA_{ill} to drop by an order of magnitude (Supplementary information), which will in turn utterly diminish the resolution enhancement. As clearly shown in Fig. 2(f) and noted from the Eqs. (2) and (3), closer the sample to the endoscope's distal end, higher will be the resolution enhancement.

Imaging demonstration of SSIE

2D surface

To demonstrate the high-resolution capability of the proposed SSIE, we image sparsely distributed fluorescent stains (Rhodamine 6G) drop-casted on a glass slide. As from the working principle of the SSIE, the speckle illumination patterns are sensitive to the distance from the sample surface (Fig. 2(d)). In this section, we experimentally verify the performance of SSIE on a 2D surface at two exemplary chosen distances of 3.7 cm and 7.2 cm. First, we depict the results obtained at focal distance of

3.7 cm (Fig. 3). The process is as follows; at the sample plane high-resolution speckles excite the fluorescent stains in the specimen. The fluorescence signal is further collected directly by the endoscopic image sensor after passing through a 580/40 nm band pass filter, placed in the imaging path. Thereafter, the super resolution image is reconstructed by using the blind-SIM algorithm. Later, for comparison, the SSIE reconstructions are compared with the standard endoscopic image without the speckle structured illumination.

In this demonstration, 120 frames of images with various speckle illimitation patterns are collected. The diffraction limited endoscopic image is obtained by summing all the 120 frames shown in Fig. 3(a). This ensures the comparison is performed with the same imaging optics. The high resolution SSIE image after the blind-SIM reconstruction is shown in Fig. 3(b). The field of view in the SSIE image as captured by the endoscopic sensor is in millimeters (Fig. 3(b)). This is orders higher than CLE's achievable limits which is typically in micrometers[17]. As expected, the SSIE image shows greatly improved resolution, so that the fine features including boundaries and edges are clearly resolved. As comparison, the stains are blurred with barely discernable edges in the diffraction limited image obtained by a standard WLE. To quantify the resolution enhancement factor of the SSIE, we performed Fourier transforms (FT) of the images in Fig. 3(a) and 3(b) and the results are shown in Fig. 3(c) and 3(d). Using Eq. (3), we obtain a resolution enhancement factor of 3.5 times and 3.39 times in the vertical direction (y) and the horizontal direction (x), respectively. This result is consistent with the expected enhancement values as shown in Fig. 2(f). Figure 3(e–g) show the zoom-in view of the object, diffraction limited image of the WLE, and the SSIE image. The resolution improvement and the sharp edges in the SSIE image is clearly visible. The optimal parameters and the number of iterations pertaining to the reconstruction makes the reconstruction accurate and the image features well defined.

From an information theory point of view, at least N^2 sub frames are needed to reconstruct super resolution image with N- fold resolution improvement. Traditional SIM uses well-known sinusoidal patterns to sample the object with high efficiency. Therefore, the oversampling factor can be very small, i.e., the total number of sub frames αN^2, where α, the oversampling factor, is close to 1. However, speckle-based blind-SIM requires more frames, i.e., $\alpha>1$, owing to the lack of knowledge of the exact illumination patterns used and the correlations between the illumination patterns. By selecting a reasonable α, the speckle-based blind-SIM is known to produce high levels of resolution indicating its robustness[9]. We explore the SSIE's performance for a secondary focal distance at 7.2 cm with 80 frames. The objective is to measure the results at a secondary focal distance to establish consensus in the results, keeping in mind that a typical endoscope has large depth of field.

The sample preparation is identical to the prior case. The enhanced image's FT (Fig. 4(d)) yields a resolution enhancement of 2.5 times and 2.39 times along vertical (y) and horizontal (x) direction, respectively, compared to its diffraction limited equivalent (Fig. 4(c)). These enhancement factors also agree well with the expected values shown in Fig. 2(e), i.e., 2.52 and 2.4 times in the y and x directions, respectively. Even with a reduced number of frames, the SSIE image (Fig. 4(b)) is well resolved, which demonstrates the robustness and reliability of the speckle approach.

3D surface

The standard WLE's are typically used for examination of the human body where the surfaces imaged are not

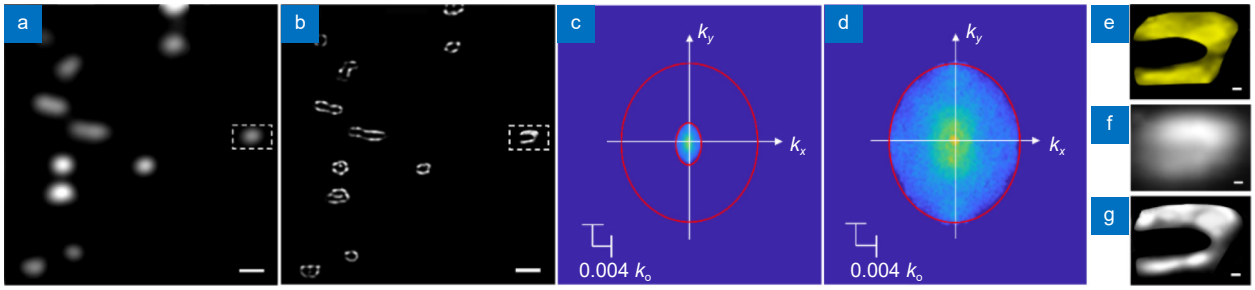

Fig. 3 | Experimental demonstration of SSIE at 3.7 cm. (**a**) Diffraction limited endoscopic image of the drop casted stains. (**b**) SSIE image of the same area in (a). Scale bars in (a-b) are 800 μm. (**c–d**) Fourier spectra of the images in (a) and (b), respectively. (**e–g**) Zoom in view of the ground truth, diffraction limited endoscopic image, and SSIE image of the marked area in (a) and (b). Scale bars in (e–g) are 100 μm.

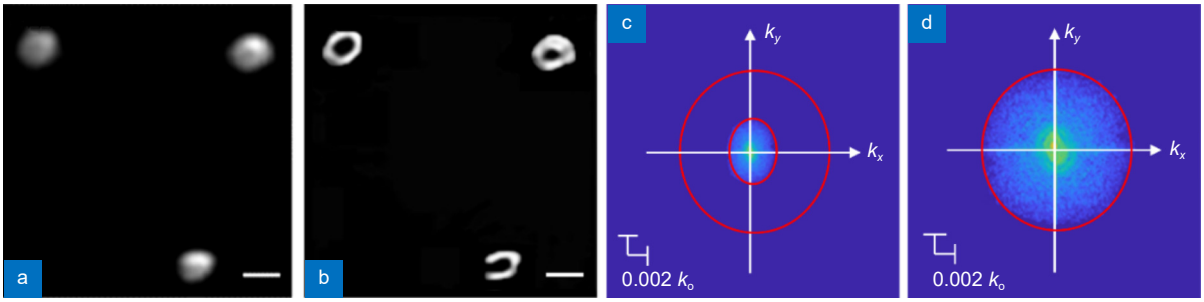

Fig. 4 | Experimental demonstration of SSIE at 7.2 cm. Diffraction limited endoscopic image (**a**) and SSIE super resolution image (**b**) of a fluorescent object. Scale bars in (a, b) are 600 um. (**c**, **d**) Fourier spectra of the images in (a) and (b), respectively.

planar, hence, we consider imaging a 3D curved nonplanar surface. One advantage of using speckle SIM is that the projected patterns remain speckles when subjected onto a 3D plane after various distortions. Because the SSIE does not need to know the illumination patterns, the reconstruction remains unaffected. Rhodamine 6G is drop casted on a curved slide as indicated in Fig. 5(a) and used as the test sample for imaging.

A set of 60 frames were used in the SSIE reconstruction. The imaging distance is around 7.2 cm. The depth of field of the sample is about 3 mm. Figure 5(b) indicates a zoom in view of the ground truth wherein the feature edges are well defined. In the diffraction limited endoscopic image (Fig. 5(c)), we observe the features are blurred, unclear and appear as a blob of a stain. This is resolved well in the SSIE image (Fig. 5(d)) at wide field of view and depth of field (see Supplementary information for more information). Since the depth of the sample varies the average resolution improvement factor is ~2.52 times in the vertical direction and ~2.2 times in the horizontal direction, which is also reasonably consistent with Fig. 2(f) for imaging distance of 7.2 cm. If we compare the two experimental results in Fig. 4 and Fig. 5, we notice the similar imaging depth, i.e., ~7.2 cm, but with a difference in number of frames (80 and 60). The resolution enhancement is comparable between the two, indicating the oversampling factor α can be reduced to less than 10 without significantly affecting the image quality. Additionally, this example demonstrates that the SSIE can be directly applied to a clinical endoscope without adjustment of focusing, where the depth of field may go up to a few millimeters. Here, the depth of field is about 3 mm, but we anticipate the depth of field can be extended much further given the endoscope's large depth of field. The prior demonstration proves and validates the concept of SSIE for 3D nonplanar surfaces where field of view and depth of field are both critical parameters along with enhanced levels of resolution. In the future, efforts will be directed into implementing the SSIE in a clinical setting, to quantize the imaging performance against the standard WLE.

Discussion

The SSIE demonstrations are independent of the internal structure, type, or specifications of the scope. Therefore, the SSIE technique can be translated into any white light endoscopic modality with similar resolution improvement factors whether its application is clinical or industrial, since the working principle remains the same (see more information in the Supplementary information, Table S1). The imaging speed of the SSIE can further be enhanced by the employment of the high-speed spatial light modulator (SLM) to control the speckle patterns (see more information in the Supplementary information). Blind-SIM reconstruction algorithm is chosen over the conventional SIM due to its robustness

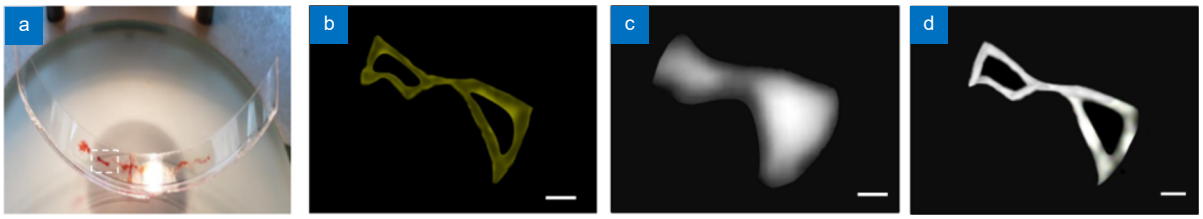

Fig. 5 | Experimental demonstrations of SSIE on curved surface with large depth of field. (**a**) Photograph of a drop casted rhodamine dye sample on a curved glass surface. (**b**) A zoom-in review of the marked area in (a) obtained from a stereo microscope. This can be considered as the ground truth of the object. Diffraction limited endoscopic image (**c**) and the SSIE image (**d**) of the same object shown in (b). Scale bars in (b–d) are 700 μm.

to the deformations of the illumination patterns which is especially important in the case of endoscopic application. The time taken for imaging is about 3 minutes for a maximum of 120 frames used in this study. Frames were acquired at a rate of one frame per second as a few milliseconds within the second timeframe are accounted for the speckle pattern to settle after the multimode fiber has been modulated. This iterative algorithm may not be fast enough for real time image reconstruction, and we use it here mainly to demonstrate the image resolution enhancement for large depth of field focus free imaging. The computational efficiency of the iterative algorithm may be optimized by employing faster GPU's. In addition, future developments along the directions of neural networks may aid in making the SSIE more inclined towards a real time application, but its tradeoffs remain to be explored[37–39].

Conclusion

In conclusion, we propose and demonstrate the SSIE, a robust, wide field and low-cost super-resolution method for applications in endoscopic practices. The concept proof experiment was conducted with a standard WLE for image acquisition and two external multi-mode fibers for delivering the speckle illumination patterns onto the subject. The performance of the SSIE being mainly limited by the illumination *NA* which decreases over distance from the endoscopic image sensor is seen to produce an enhancement of 2–4.5 times the WLE equivalent based on the focal distances considered. SSIE greatly extends the spatial resolution with a cost of increased number of measurements. However, the time for data acquisition can be greatly reduced by implementing high speed imaging (Supplementary information). Since the endoscope requires no focusing, imaging objects with significant depth becomes rather straightforward and the speckle-based approach compliments the reconstruction efforts against possible distortions as otherwise is observed when utilizing traditional SIM against such objects. With respect to the setup, the SSIE is greatly simplified compared to other high definition or ultra-high-definition endoscopy techniques. Additionally, the SSIE does not rely on any specific properties of the specimen or sample, therefore any sample can be used. In the future, we anticipate that the SSIE will transform the standard white light endoscope into a much more accurate imaging tool, leading to profound benefits to the GI endoscopic community and the patient.

Materials and methods

The experimental demonstration of the SSIE took frames equal to and lower than 120 (1 frame per second) to generate data's (Figs. 3, 4, 5). The fluorescent signal is collected by the endoscopic lens with a band pass filter (580/40 nm). The wide field of view image reconstruction takes about three minutes on a desktop computer with GTX 1080Ti graphics card and a i7-8700k. All experiments were conducted by using the white light Teslong's Borescope Endoscope. The dye used was Rhodamine 6G which was diluted against ethanol at 8 mg/mL concentration. This is drop casted on a glass slide using a pipette. The US air force target utilized was that of the Edmunds USAF resolution target, pocket size. The microscope used to establish ground truth was, Olympus IX83, with 50× magnification, 0.5 NA and Olympus SZ40, with the eyepiece 20×, objective: zoom lens 0.6-4× (stereo microscope). The multimode fibers used were from Thorlabs (0.22 NA, High-OH, 50 μm core, Lambda: 250–1200 nm, FC/APC termination). The laser utilized is the Newport, continuous wave, power 200 mW and the corresponding neutral density filters used in the light path was from Thorlabs (lower than two orders of attenuation). The fiber beam splitter used was from OZ optics (50/50 beam split ratio).

References

1. Lopez-Ceron M, van den Broek FJC, Mathus-Vliegen EM, Boparai KS, van Eeden S et al. The role of high-resolution endoscopy and narrow-band imaging in the evaluation of upper GI neoplasia in familial adenomatous polyposis. *Gastrointest Endosc* **77**, 542–550 (2013).
2. Anagnostopoulos GK, Yao K, Kaye P, Fogden E, Fortun P et al. High-resolution magnification endoscopy can reliably identify normal gastric mucosa, *Helicobacter pylori*-associated gastritis, and gastric atrophy. *Endoscopy* **39**, 202–207 (2007).
3. Bruno MJ. Magnification endoscopy, high resolution endoscopy, and chromoscopy; towards a better optical diagnosis. *Gut* **52**, iv7–iv11 (2003).
4. Rust MJ, Bates M, Zhuang XW. Sub-diffraction-limit imaging by stochastic optical reconstruction microscopy (STORM). *Nat Methods* **3**, 793–796 (2006).
5. Hess ST, Girirajan TPK, Mason MD. Ultra-high resolution imaging by fluorescence photoactivation localization microscopy. *Biophys J* **91**, 4258–4272 (2006).
6. Hell SW, Wichmann J. Breaking the diffraction resolution limit by stimulated emission: stimulated-emission-depletion fluorescence microscopy. *Opt Lett* **19**, 780–782 (1994).
7. Gustafsson MGL. Surpassing the lateral resolution limit by a factor of two using structured illumination microscopy. *J Microsc* **198**, 82–87 (2000).
8. Heintzmann R, Jovin TM, Cremer C. Saturated patterned excitation microscopy: a concept for optical resolution improvement. *J Opt Soc Am A* **19**, 1599–1609 (2002).

9. Lee YU, Zhao JX, Ma Q, Khorashad LK, Posner C et al. Metamaterial assisted illumination nanoscopy via random super-resolution speckles. *Nat Commun* **12**, 1559 (2021).
10. Liu ZW. Plasmonics and metamaterials based super-resolution imaging (Conference Presentation). *Proc SPIE* **10194**, 101940M (2017).
11. Wei FF, Liu ZW. Plasmonic structured illumination microscopy. *Nano Lett* **10**, 2531–2536 (2010).
12. Fernández-Domínguez AI, Liu ZW, Pendry JB. Coherent four-fold super-resolution imaging with composite photonic–plasmonic structured illumination. *ACS Photonics* **2**, 341–348 (2015).
13. Goetz M, Watson A, Kiesslich R. Confocal laser endomicroscopy in gastrointestinal diseases. *J Biophotonics* **4**, 498–508 (2011).
14. Jabbour JM, Saldua MA, Bixler JN, Maitland KC. Confocal endomicroscopy: instrumentation and medical applications. *Ann Biomed Eng* **40**, 378–397 (2012).
15. Elliott AD. Confocal microscopy: principles and modern practices. *Curr Protoc Cytom* **92**, e68 (2020).
16. Ilie MA, Caruntu C, Lupu M, Lixandru D, Tampa M et al. Current and future applications of confocal laser scanning microscopy imaging in skin oncology. *Oncol Lett* **17**, 4102–4111 (2019).
17. Meining A, Saltzman JR, Travis AC. Confocal laser endomicroscopy and endocytoscopy (2020). https://www.uptodate.com/contents/confocal-laser-endomicroscopy-and-endocytoscopy
18. Chang Tou Pin et al. Probe-based confocal laser endomicroscopy: an evaluation of its role towards real-time, in vivo, in situ intraoperative applications. Imperial College London (2016).
19. Wijsmuller AR, Ghnassia JP, Varatharajah S, Schaeffer M, Leroy J et al. Prospective trial on probe-based confocal laser endomicroscopy for the identification of the distal limit in rectal adenocarcinoma. *Surg Innov* **25**, 313–322 (2018).
20. Singh H, Schiff GD, Grabe ML, Igho O, Thompson MJ. The global burden of diagnostic errors in primary care. *BMJ Qual Saf* **26**, 484–494 (2016).
21. Kurniawan N, Keuchel M. Flexible gastro-intestinal endoscopy clinical challenges and technical achievements. *Comput Struct Biotechnol J* **15**, 168–179 (2017).
22. Moore LE. The advantages and disadvantages of endoscopy. *Clin Tech Small Anim Pract* **18**, 250–253 (2003).
23. Banerjee R, Reddy DN. Advances in endoscopic imaging: advantages and limitations. *J Dig Endosc* **3**, 7–12 (2012).
24. ASGE Technology Committee, Chauhan SS, Dayyeh BKA, Bhat YM, Gottlieb KT et al. Confocal laser endomicroscopy. *Gastrointest Endosc* **80**, 928–938 (2014).
25. Mudry E, Belkebir K, Girard J, Savatier J, Le Moal E et al. Structured illumination microscopy using unknown speckle patterns. *Nat Photonics* **6**, 312–315 (2012).
26. Yeh LH, Chowdhury S, Repina NA, Waller L. Speckle-structured illumination for 3D phase and fluorescence computational microscopy. *Biomed Opt Express* **10**, 3635–3653 (2019).
27. Yeh LH, Chowdhury S, Waller L. Computational structured illumination for high-content fluorescence and phase microscopy. *Biomed Opt Express* **10**, 1978–1998 (2019).
28. Ponsetto JL, Wei FF, Liu ZW. Localized plasmon assisted structured illumination microscopy for wide-field high-speed dispersion-independent super resolution imaging. *Nanoscale* **6**, 5807–5812 (2014).
29. Min JH, Jang J, Keum D, Ryu SW, Choi C et al. Fluorescent microscopy beyond diffraction limits using speckle illumination and joint support recovery. *Sci Rep* **3**, 2075 (2013).
30. Kim M, Park C, Rodriguez C, Park Y, Cho YH. Superresolution imaging with optical fluctuation using speckle patterns illumination. *Sci Rep* **5**, 16525 (2015).
31. Ayuk R, Giovannini H, Jost A, Mudry E, Girard J et al. Structured illumination fluorescence microscopy with distorted excitations using a filtered blind-SIM algorithm. *Opt Lett* **38**, 4723–4726 (2013).
32. Hoffman ZR, DiMarzio CA. Structured illumination microscopy using random intensity incoherent reflectance. *J Biomed Opt* **18**, 061216 (2013).
33. Chaigne T, Gateau J, Allain M, Katz O, Gigan S et al. Super-resolution photoacoustic fluctuation imaging with multiple speckle illumination. *Optica* **3**, 54–57 (2016).
34. García J, Zalevsky Z, Fixler D. Synthetic aperture super resolution by speckle pattern projection. *Opt Express* **13**, 6073–6078 (2005).
35. Clancy NT, Li R, Rogers K, Driscoll P, Excel P et al. Development and evaluation of a light-emitting diode endoscopic light source, advanced biomedical and clinical diagnostic systems. *Proc SPIE* **8214**, 82140R (2012).
36. ASGE Technology Committee, Varadarajulu S, Banerjee S, Barth BA, Desilets DJ et al. GI endoscopes. *Gastrointest Endosc* **74**, 1–6.e6 (2011).
37. Waddington DEJ, Hindley N, Koonjoo N, Chiu C, Reynolds T et al. On real-time image reconstruction with neural networks for MRI-guided radiotherapy. arXiv: 2202.05267 (2022). https://doi.org/10.48550/arXiv.2202.05267
38. Wu DF, Kim K, Li QZ. Computationally efficient deep neural network for computed tomography image reconstruction. *Med Phys* **46**, 4763–4776 (2019).
39. Paderno A, Gennarini F, Sordi A, Montenegro C, Lancini D et al. Artificial intelligence in clinical endoscopy: Insights in the field of videomics. *Front Surg* **9**, 933297 (2022).

Acknowledgements

This work was partially supported by the Gordon and Betty Moore Foundation Grant No. 5722. The authors would like to thank Junxiang Zhao (Department of Electrical and Computer Engineering, UCSD) for helping to buy the required components and for helping assemble the components. The authors would also like to thank Abhijith Karkisaval Ganapati (Department of Bioengineering, UCSD) for providing access and knowledge on the stereo microscope used at Professor Ratnesh Lal's laboratory (Bioengineering, UCSD). The authors would like to acknowledge Dr. Samuel Marcus for useful discussions.

Author contributions

E. Abraham and Z. W. Liu produced the idea. E. Abraham and J. X. Zhou did the theory part. E. Abraham did the experiments. E. Abraham and J. X. Zhou prepared the figures. E. Abraham prepared the paper. Z. W. Liu supervised the overall project.

Competing interests

The authors declare no competing financial interests.

Supplementary information

Supplementary information for this paper is available at https://doi.org/10.29026/oea.2023.220163